SUPPLEMENTAL DATA

Production of recombinant proteins – ApoA-I protein variants expression and purification by Ni-affinity chromatography, removal of the N-terminal His tag by reaction with TEV protease and final Ni-affinity chromatography purification were performed as described (1, 2). Protein purity was confirmed by SDS-PAGE and protein samples were stored frozen in 6 M guanidine chloride buffer until use. Before experiments, stored proteins were refolded from 6 M guanidine chloride by extensive dialysis against the appropriate experiment-specific buffer. After refolding, protein concentration was determined spectrophotometrically (ε_{280} = 1.13 $(mg/ml)^{-1}$ cm^{-1} (3) and by the BCA assay (Pierce).

Denaturing gel electrophoresis (SDS-PAGE) – 3 μg of protein in SDS and β-mercaptoethanol buffer were boiled for 20 min, loaded per lane of 4-20% Tris-glycine gels (Novex™, Invitrogen), and run at 125 V for 2 h in SDS-Tris-glycine buffer. Gels were stained with GelCode™ blue stain reagent (Thermo Scientific).

Non-denaturing gradient gel electrophoresis (NDGGE) – Novex™ 4–20% Tris-glycine gels (Life Technologies) were loaded with 3 μg of protein per lane and run to termination as described (4). Staining by GelCode™ blue stain reagent (Thermo Scientific) and imaging were performed as previously described (5).

ABCA1-mediated cellular cholesterol release – RAW264.7 macrophages were dispensed into a 48-well plate at $3x10^5$ cell per well, suspended in 0.4 ml of high-glucose (4.5 g/l) DMEM (Sigma AQmedia, with L-Ala-L-Gln, $NaHCO_3$, and pyridoxine), 50 μg/ml gentamicin and 10% FBS. After 48 h, the cells were labeled with TopFluor cholesterol by 1 h incubation with 0.025 mM TopFluor cholesterol, 0.10 mM unlabeled cholesterol, 10 mM methyl-β-cyclodextrin, and 1 μg/ml ACAT inhibitor (Sandoz 58-035, Sigma-Aldrich) in MEM-HEPES medium (10 mM HEPES, pH 7.4). Cells were washed with MEM-HEPES and incubated in 0.25 ml of high-glucose (4.5 g/l) DMEM, 50 μg/ml gentamicin, 0.2 % BSA, 2 μg/ml ACAT inhibitor and 0.3 mM Cpt-cAMP (Abcam) for 18 h. After removing the medium, the TopFluor cholesterol labeled cells were incubated with apoA-I samples (1.0-2.5 μg/ml) in the incubation medium (MEM-HEPES buffer (10 mM, pH 7.4) with 2 μg/ml ACAT inhibitor and 0.15 mM Cpt-cAMP) for 4 h at 37 °C and TopFluor cholesterol fluorescence of the incubation medium was measured (ex 482 nm, em 515 nm) on a BioTek Synergy H1 microplate reader. Background fluorescence intensity of the incubation medium and background cholesterol release were subtracted from the cell culture medium readings. Background cholesterol release (always < 2%) was measured in the medium of cells incubated in the absence of apoA-I. TopFluor cholesterol released from cells into the medium was expressed as percentage of initial total TopFluor cholesterol, defined as the TopFluor cholesterol fluorescence extracted from the labeled cells with 0.25 ml of 1% cholic acid (≥ 6 wells per experiment). Under these experimental conditions, cholesterol release to non-oxidized wild-type apoA-I (wt-ApoA-I) was 6.2±0.5 % and 15.3±1.0 % ($n \geq 12$), for 1.0 and 2.5 μg/ml non-oxidized wt-ApoA-I, respectively. In the absence of pre-incubation with Cpt-cAMP, cholesterol release to non-oxidized wt-ApoA-I was always

below 0.5 %, indicating that in standard experimental conditions (pre-incubation with Cpt-cAMP), cholesterol release is mainly mediated by ABCA1.

Transmission electron microscopy – Protein samples were adsorbed onto freshly glow discharged carbon-coated copper grids for 1 minute, the sample excess was then removed with filter paper. The grids were stained with 1% (w/v) uranyl acetate for 30 s. Images were taken between 11000 and 52000 x magnification using a Tecnai T12 transmission electron microscope (FEI; Hillsboro, OR) operating at 120 kV and equipped with an UltraScan 1000 CCD camera (Gatan; Pleasanton, CA) (6, 7).

Supplemental Table S1

Peptide	CE *V*	Precursor *m/z*	Product *m/z*		HPLC r.t. *min*
QEM[+16.0]SK.light	10.9 17	319.6443	234.1448 129.0659	y2 + b1 +	1.09
QEM[+16.0]SK.heavy	10.9 17	323.6514	242.159 129.0659	y2 + b1 +	1.09
QEMSK.light	10.7 17	311.6469	234.1448 129.0659	y2 + b1 +	2.84
QEMSK.heavy	10.7 17	315.654	242.159 129.0659	y2 + b1 +	2.84
WQEEM[+16.0]ELYR.light	21 21 25	650.2873	985.4295 315.1452 204.1131	y7 + b2 + c1 +	4.82
WQEEM[+16.0]ELYR.heavy	21 21 25	653.7959	992.4467 315.1452 204.1131	y7 + b2 + c1 +	4.82
WQEEMELYR.light	20.9 21 25	642.2899	969.4346 315.1452 204.1131	y7 + b2 + c1 +	5.38
WQEEMELYR.heavy	20.9 21 25	645.7985	976.4518 315.1452 204.1131	y7 + b2 + c1 +	5.38
LSPLGEEM[+16.0]R.light	17.3 20 14	524.2606	847.3978 637.261 424.2026	y4 ++ y2 + b1 +	4.41
LSPLGEEM[+16.0]R.heavy	17.3 20 14	527.7692	854.415 637.261 427.7111	y4 ++ y2 + b1 +	4.41
LSPLGEEMR.light	14 23 14	516.2631	831.4029 621.2661 416.2051	y4 ++ y2 + b1 +	4.95
LSPLGEEMR.heavy	14 23 14	519.7717	838.4201 621.2661 419.7137	y4 ++ y2 + b1 +	4.95
AELQEGAR.light	12 14.6 12	437.2249	673.3628 560.2787 337.185	y6 + y5 + y6 ++	3.45

Supplemental Table S1. Identity, precursor/product mass, collision energy and HPLC retention time for peptides and transitions used for determination of the degree of Met oxidation in wt-ApoA-I by LC-MS.

Supplemental Table S2

Sample Name	Concentration mg/ml	Time after heating	Major Peak V_e (ml)	Major Peak K_{av}
60C-4WF-ApoA-I (Tetramer)*	1.0	~15 min	13.0	0.33
90C-wt-ApoA-I	1.0	~24 h at 4 °C	13.5	0.38
Non-oxidized wt-ApoA-I	1.0	N/A	13.8	0.40
MPO-3:1-H_2O_2-wt-ApoA-I (Shoulder)	1.0	N/A	14.0	0.42
90C-wt-ApoA-I	1.0	~15 min	14.4	0.45
H_2O_2-wt-ApoA-I	1.0	N/A	14.6	0.47
MPO-3:1-H_2O_2-wt-ApoA-I (Monomer)	1.0	N/A	14.7	0.47
Non-oxidized wt-ApoA-I	0.1	N/A	14.8	0.48
H_2O_2-wt-ApoA-I	0.1	N/A	14.8	0.48
60C-4WF-ApoA-I (Monomer)*	1.0	~15 min	14.9	0.49
MPO-10:1-H_2O_2-wt-ApoA-I (Monomer)	1.0	N/A	15.0	0.50

Supplemental Table S2. SEC elution volumes (V_e) and distribution coefficients (K_{av}) of apoA-I samples (See Fig. 4 and supplemental Fig. S2).
* 4WF-ApoA-I incubated at 60 °C for 1 h (60C-4WF-ApoA-I) was previously characterized as forming predominantly tetramers by dynamic light scattering (4).

Supplemental Table S3

Sample Name	Seeds %	Aggregation yield (%)
H_2O_2-wt-ApoA-I	N/A	91.3 ± 3.4 (*n*=6)
Non-oxidized wt-ApoA-I + H_2O_2-wt-ApoA-I amyloid fibrils (seeds)	10	55.0 ± 4.9 (*n*=6)
	1	45.6 ± 17.5 (*n*=3)

Supplemental Table S3. Yield of H_2O_2-wt-ApoA-I aggregation upon 6 days incubation under fibrillation conditions and yield of non-oxidized apoA-I aggregation upon 20 days seeding with pre-formed H_2O_2-wt-ApoA-I amyloid-like fibrils (10 or 1%). Residual soluble protein in the supernatant of fibrillation samples was measured by BCA and compared to the protein concentration before fibrillation. The initial concentration of the seeded fibrillation samples was assumed to be the concentration of the non-oxidized wt-ApoA-I alone.

Supplemental Fig. S1

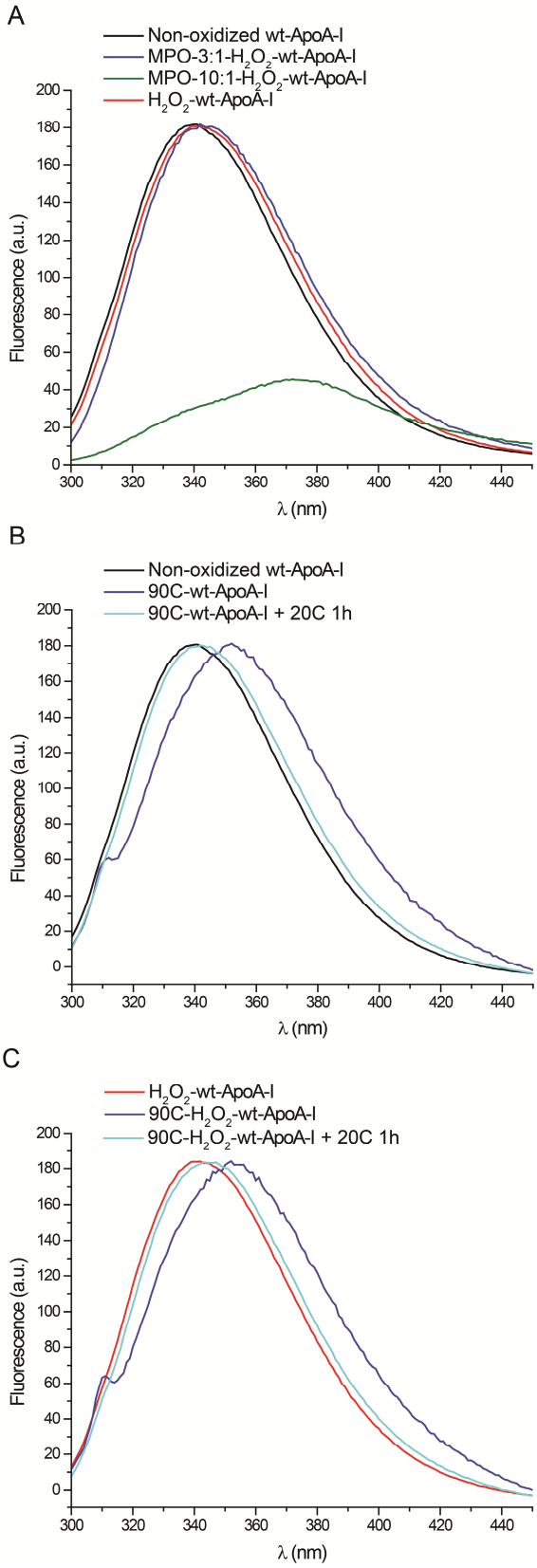

Supplemental FIGURE S1. Fluorescence emission analysis of non-oxidized and oxidized apoA-I samples at 50 µg/ml in iPBS. Excitation wavelength was 280 nm. Panel A: apoA-I samples oxidized with different methods. Panel B and C: heating/cooling of non-oxidized- and H_2O_2-ApoA-I, respectively. "90C-wt-ApoA-I + 20C 1h" and "90C-H_2O_2-ApoA-I + 20C 1h" samples were heated at 90 °C for 1h and then incubated at 20 °C for 1 h before fluorescence analysis.

Supplemental Fig. S2

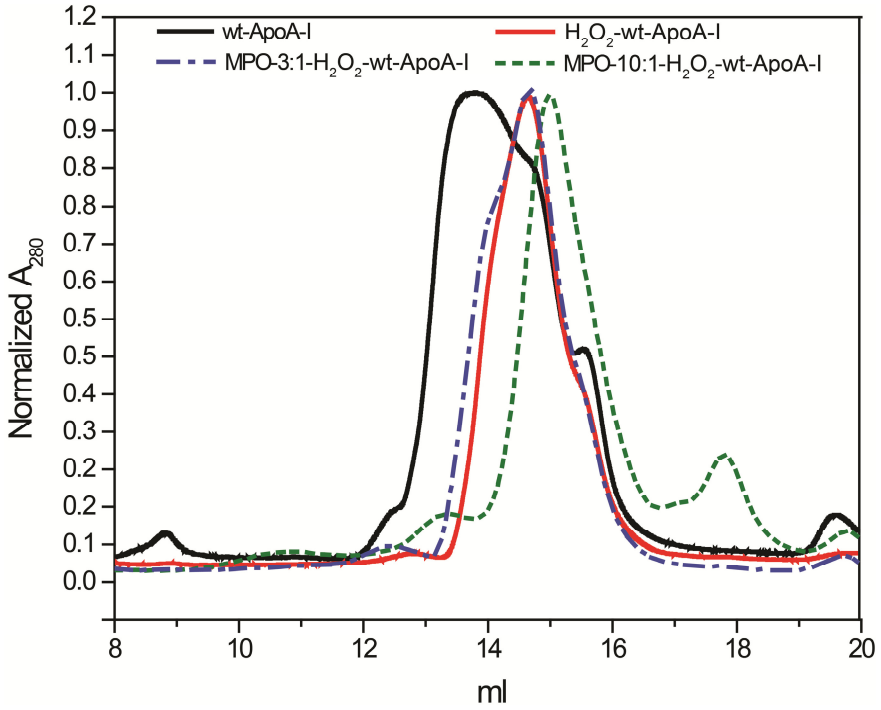

Supplemental FIGURE S2. SEC analysis of 100 µl of apoA-I samples at 1.0 mg/ml in iPBS. To facilitate the comparison of different chromatograms, the y-axes were manually adjusted to normalize the intensity of the most prominent peak in each chromatogram to 1.

Supplemental Fig. S3

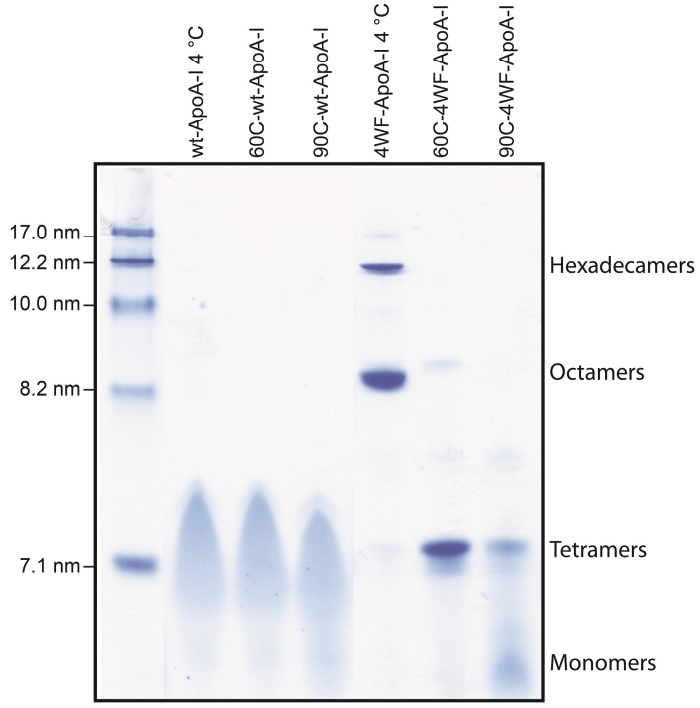

Supplemental FIGURE S3. NDGGE analysis of heated apoA-I samples (wt-ApoA-I and 4WF-ApoA-I). Protein samples at 1.0 mg/ml were incubated for 1 h at 60 or 90 °C (60C- and 90C- labels, respectively). After cooling at room temperature for 10 min, samples were loaded on gel (3 µg/lane). Molecular weight markers were High Molecular Weight Calibration Kit (GE Healthcare). Note: although similar results were already published by our group (4), this NDGGE analysis was replicated and presented here as a reference to facilitate interpretation of Fig. 5 in the main paper.

Supplemental Fig. S4

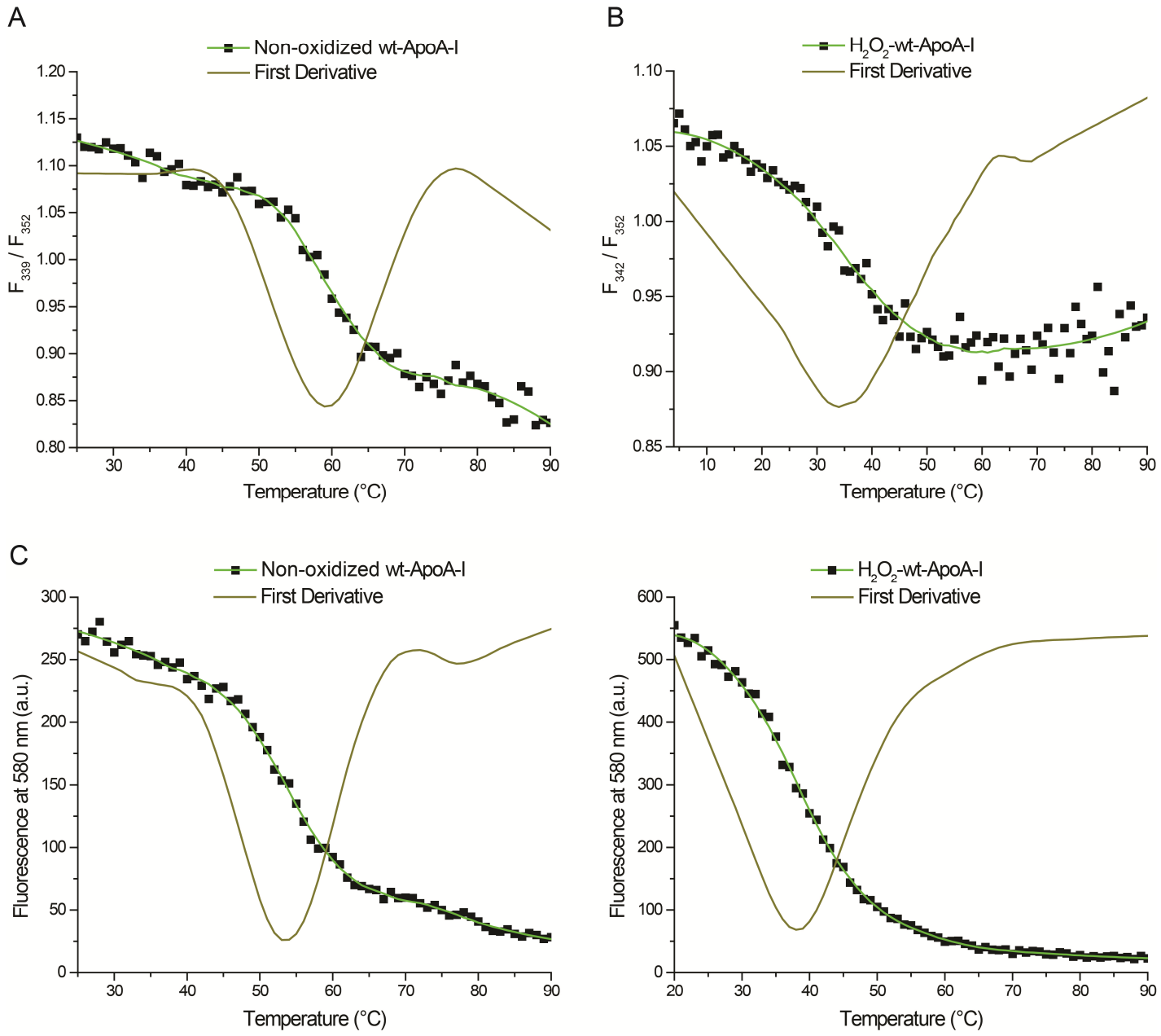

Supplemental FIGURE S4. Representative melting curves of non-oxidized- (panel A and C) and H_2O_2-ApoA-I (panel B and D). Thermal shift analysis was performed by two independent methods: using temperature-dependent changes in Trp fluorescence (ex 295 nm) (panel A and B) and SYPRO orange fluorescence (ex 492 nm) (panel C and D) as reporter signals (see *Materials and Methods*). In panels A and B, the values reported are Trp F_{WMF} (F) / F_{WMF} (U), as defined in *Materials and Methods*.

Supplemental Fig. S5

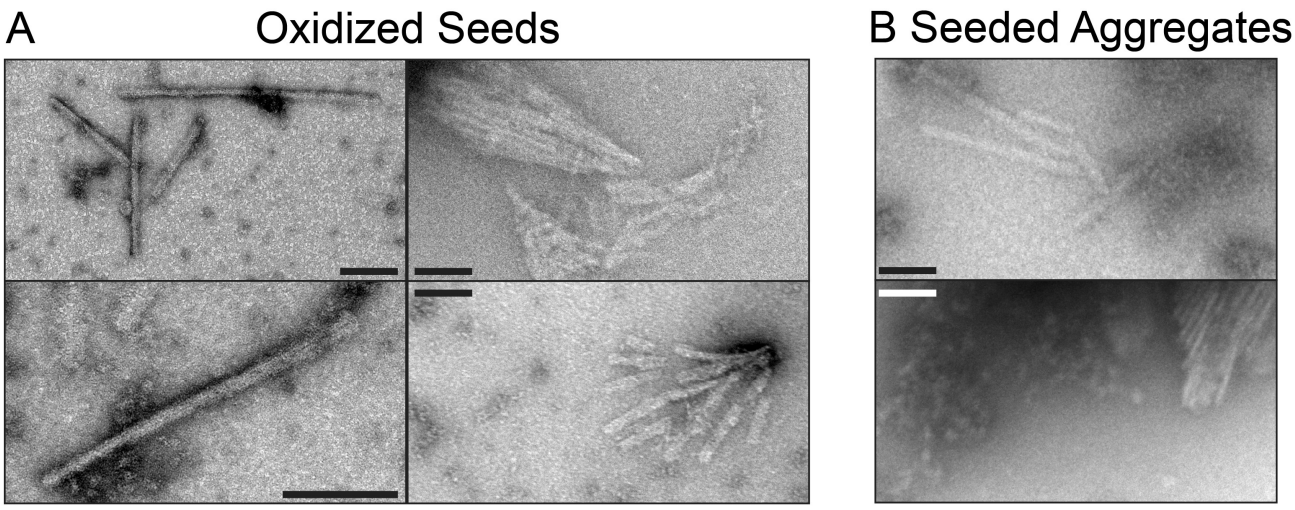

Supplemental FIGURE S5. EM analysis of H_2O_2-ApoA-I seeds (panel A) and seeded non-oxidized apoA-I aggregates (panel B). Negative staining EM analysis was performed on H_2O_2-ApoA-I seeds after 4 days under fibrillation conditions (panel A) and on non-oxidized apoA-I seeded with 10% H_2O_2-ApoA-I seeds and incubated for 20 days under fibrillation conditions (panel B). For each sample, two micrographs of different grid areas are reported at the top and bottom of each column. Two independent samples are reported in panel A, left and right columns. These images illustrate well the variability in morphology typical of Met-oxidized apoA-I amyloid fibrils (2, 8). Bars in figure represent 100 nm markers.

Supplemental Fig. S6

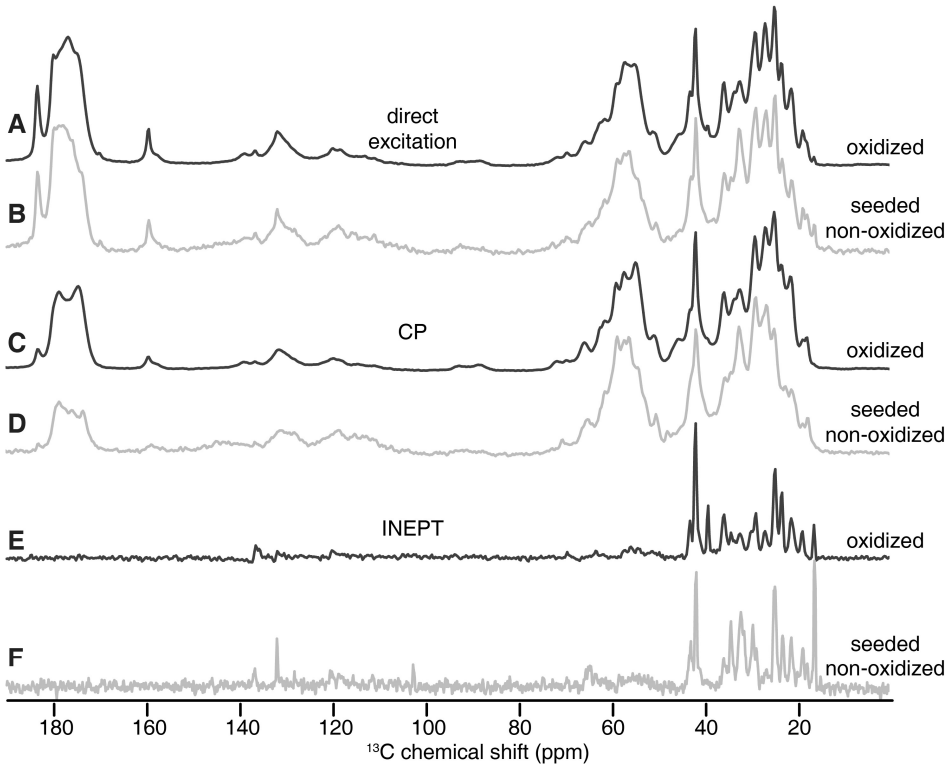

Supplemental FIGURE S6. 1D MAS NMR spectra of [U-^{13}C,^{15}N] apoA-I. (A-B) direct excitation ^{13}C, (C-D) ^{1}H-^{13}C CP, and (E-F) ^{1}H-^{13}C refocused INEPT spectra. Aggregates of H_2O_2-wt-^{13}C,^{15}N-ApoA-I and aggregates of non-oxidized wt-^{13}C,^{15}N-ApoA-I seeded with unlabeled pre-aggregated H_2O_2-wt-ApoA-I are reported in black (A, C, E) and gray (B, D, F), respectively.

Supplemental Fig. S7

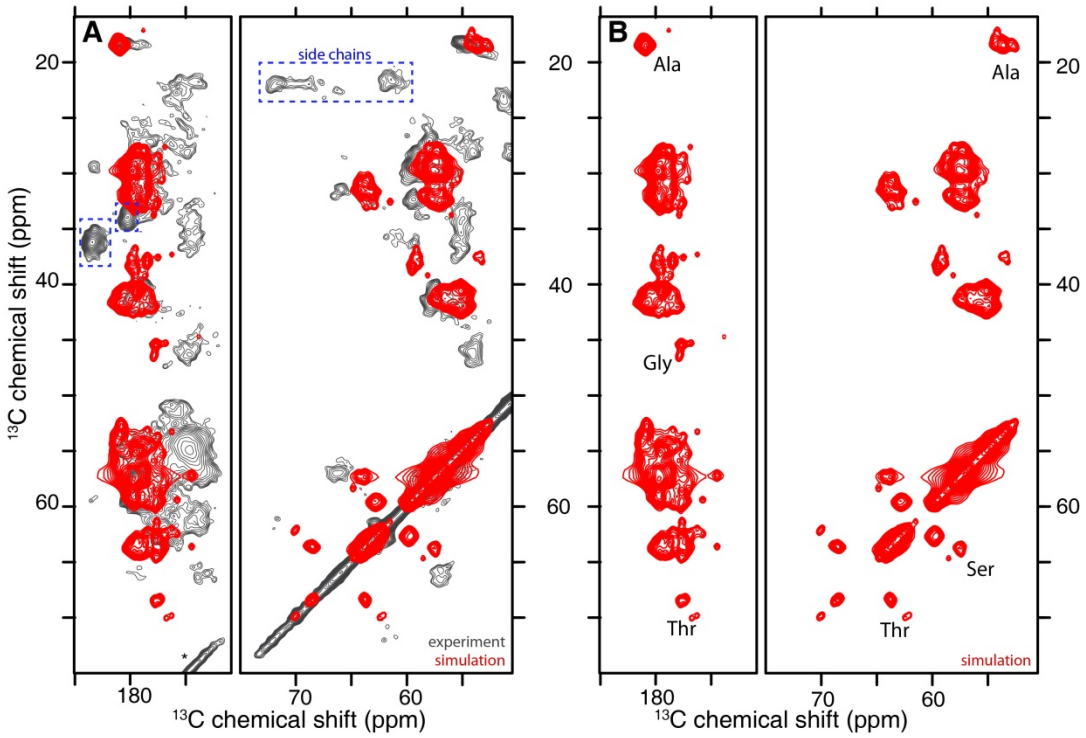

Supplemental FIGURE S7. Comparison of the experimental MAS NMR 2D spectrum of wt-^{13}C,^{15}N-ApoA-I aggregates to a simulated prediction based on the X-ray-determined α-helical native structure of C-terminal truncated Delta(185-243)-ApoA-I (9). (A) Overlay of experimental and simulated data. (B) Simulation by itself. Since the ^{13}C chemical shift prediction with the SPARTA+ program (10) is limited to backbone and Cβ carbons, only part of the spectrum is shown. Colored boxes mark side chain peaks visible in the experimental data that were not simulated.

Supplemental Fig. S8

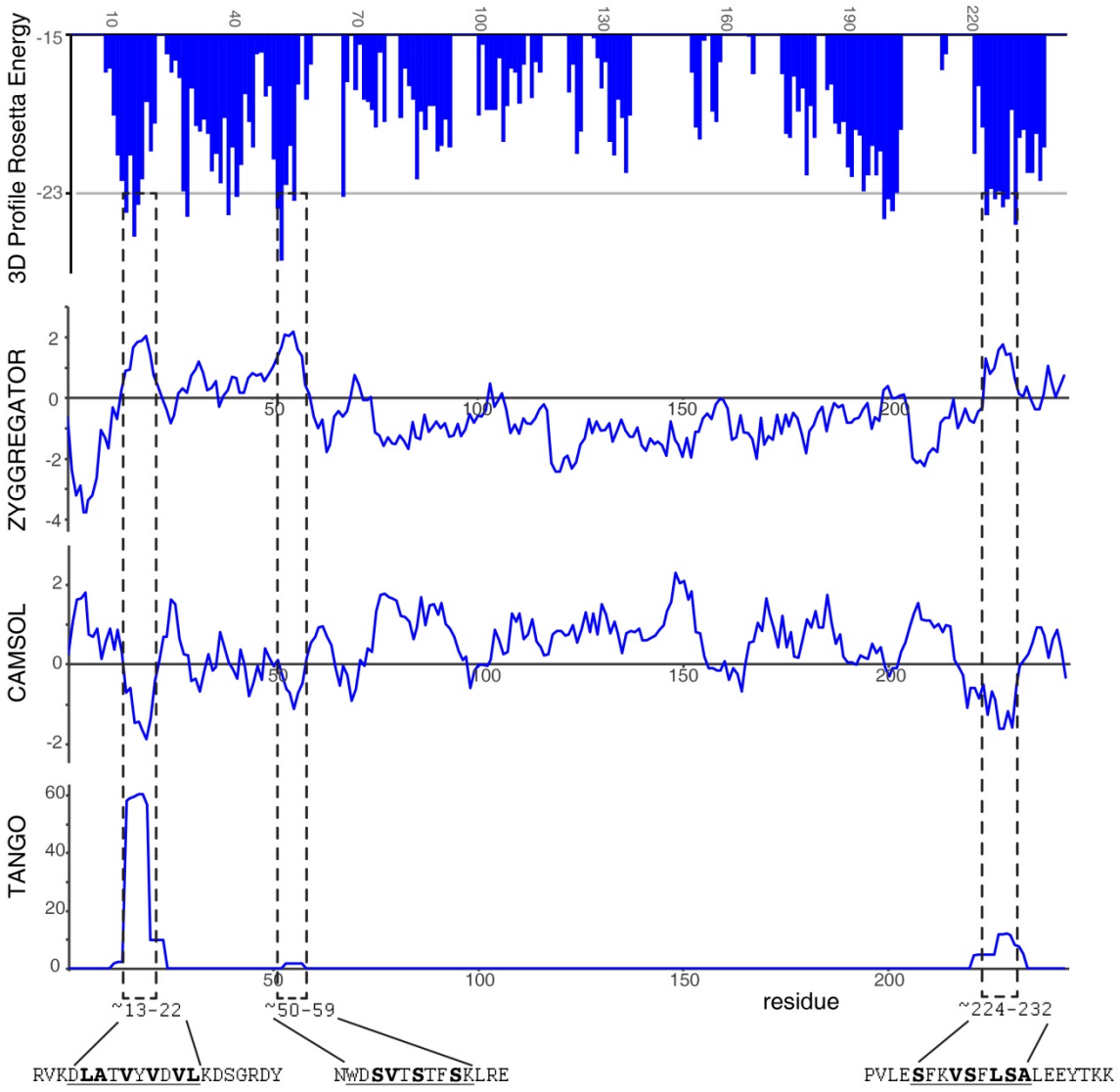

Supplemental FIGURE S8. Amyloid-propensity prediction results. The apoA-I sequence was analyzed for amyloid and aggregation propensity using four algorithms: 3D Profile (via ZipperDB) (11), Zyggregator (12), CamSol (13), and TANGO (14). The sequence areas that appear to be consensus elements with high predicted amyloidogenicity are indicated with dashed boxes. The approximate sequence positions (underlined residues), with their primary sequence context, are indicated at the bottom. In the sequence, β-sheet residues detected by ssNMR are shown in bold.

REFERENCES

1. Tubb, M. R., Smith, L. E., and Davidson, W. S. (2009) Purification of recombinant apolipoproteins A-I and A-IV and efficient affinity tag cleavage by tobacco etch virus protease. *J. Lipid Res.* **50**, 1497-1504
2. Chan, G. K., Witkowski, A., Gantz, D. L., Zhang, T. O., Zanni, M. T., Jayaraman, S., and Cavigiolio, G. (2015) Myeloperoxidase-mediated Methionine Oxidation Promotes an Amyloidogenic Outcome for Apolipoprotein A-I. *J. Biol. Chem.* **290**, 10958-10971
3. Rogers, D. P., Roberts, L. M., Lebowitz, J., Datta, G., Anantharamaiah, G. M., Engler, J. A., and Brouillette, C. G. (1998) The lipid-free structure of apolipoprotein A-I: effects of amino-terminal deletions. *Biochemistry* **37**, 11714-11725
4. Jayaraman, S., Abe-Dohmae, S., Yokoyama, S., and Cavigiolio, G. (2011) Impact of self-association on function of apolipoprotein A-I. *J. Biol. Chem.* **286**, 35610-35623
5. Cavigiolio, G., Shao, B., Geier, E. G., Ren, G., Heinecke, J. W., and Oda, M. N. (2008) The interplay between size, morphology, stability, and functionality of high-density lipoprotein subclasses. *Biochemistry* **47**, 4770-4779
6. Boatz, J. C., Whitley, M. J., Li, M., Gronenborn, A. M., and van der Wel, P. C. A. (2017) Cataract-associated P23T gammaD-crystallin retains a native-like fold in amorphous-looking aggregates formed at physiological pH. *Nat Commun* **8**, 15137
7. Lin, H. K., Boatz, J. C., Krabbendam, I. E., Kodali, R., Hou, Z., Wetzel, R., Dolga, A. M., Poirier, M. A., and van der Wel, P. C. A. (2017) Fibril polymorphism affects immobilized non-amyloid flanking domains of huntingtin exon1 rather than its polyglutamine core. *Nat Commun* **8**, 15462
8. Wong, Y. Q., Binger, K. J., Howlett, G. J., and Griffin, M. D. (2010) Methionine oxidation induces amyloid fibril formation by full-length apolipoprotein A-I. *Proc. Natl. Acad. Sci. U. S. A.* **107**, 1977-1982
9. Mei, X., and Atkinson, D. (2011) Crystal structure of C-terminal truncated apolipoprotein A-I reveals the assembly of high density lipoprotein (HDL) by dimerization. *The Journal of biological chemistry* **286**, 38570-38582
10. Shen, Y., and Bax, A. (2010) SPARTA+: a modest improvement in empirical NMR chemical shift prediction by means of an artificial neural network. *J. Biomol. NMR* **48**, 13-22
11. Goldschmidt, L., Teng, P. K., Riek, R., and Eisenberg, D. (2010) Identifying the amylome, proteins capable of forming amyloid-like fibrils. *Proc. Natl. Acad. Sci. U. S. A.* **107**, 3487-3492
12. Tartaglia, G. G., and Vendruscolo, M. (2008) The Zyggregator method for predicting protein aggregation propensities. *Chem Soc Rev* **37**, 1395-1401
13. Sormanni, P., Aprile, F. A., and Vendruscolo, M. (2015) The CamSol Method of Rational Design of Protein Mutants with Enhanced Solubility. *J. Mol. Biol.* **427**, 478-490
14. Fernandez-Escamilla, A.-M., Rousseau, F., Schymkowitz, J., and Serrano, L. (2004) Prediction of sequence-dependent and mutational effects on the aggregation of peptides and proteins. *Nat. Biotechnol.* **22**, 1302-1306